Effect of Hydrocarbon Chain Length of Disubstituted Triphenyl-amine-Based Organic Dyes on Dye-Sensitized Solar Cells

ARTICLE *in* THE JOURNAL OF PHYSICAL CHEMISTRY C · OCTOBER 2011

Impact Factor: 4.77 · DOI: 10.1021/jp2054519

7 AUTHORS, INCLUDING:

Jin-Yun Liao
University of Texas at Austin
29 PUBLICATIONS **1,194** CITATIONS
SEE PROFILE

Yong Shen
Sun Yat-Sen University
55 PUBLICATIONS **690** CITATIONS
SEE PROFILE

Dai-Bin Kuang
Sun Yat-Sen University
111 PUBLICATIONS **5,856** CITATIONS
SEE PROFILE

THE JOURNAL OF PHYSICAL CHEMISTRY C

ARTICLE

pubs.acs.org/JPCC

Effect of Hydrocarbon Chain Length of Disubstituted Triphenyl-amine-Based Organic Dyes on Dye-Sensitized Solar Cells

Qiong-Yan Yu,[†] Jin-Yun Liao,[†] Shi-Ming Zhou,[†] Yong Shen,[†] Jun-Min Liu,[*,†] Dai-Bin Kuang,[†] and Cheng-Yong Su[*,†,‡]

[†]MOE Laboratory of Bioinorganic and Synthetic Chemistry/KLGHEI of Environment and Energy Chemistry, State Key Laboratory of Optoelectronic Materials and Technologies, School of Chemistry and Chemical Engineering, Sun Yat-Sen University, Guangzhou, 510275, China

[‡]State Key Laboratory of Applied Organic Chemistry, Lanzhou University, Lanzhou 730000, China

Supporting Information

ABSTRACT: Three organic dyes incorporating a disubstituted triphenyl-amine unit as the electron donor, a thiophene moiety as the conjugated spacer, and 2-cyanoacrylic acid as the electron acceptor, have been synthesized and applied for the dye-sensitized solar cells (DSSCs). The conversion efficiencies of the DSSCs range from 4.99 to 6.04%. The influence of the hydrophobic hydrocarbon chain length of the substituent group in these dyes on the device performance in DSSCs has been investigated. It was found that the dyes with longer hydrocarbon chains gave higher photocurrents, open-circuit voltages, and efficiency values, which may derive from the higher molar absorption coefficient of metal-to-ligand charge transfer (MLCT), more appropriate localization of the frontier orbitals and longer electron lifetimes. We attribute the importance of the lengthening of the anchoring groups to the role of the dye as a better absorber for the incoming light and longer blocking layer to avoid charge recombination.

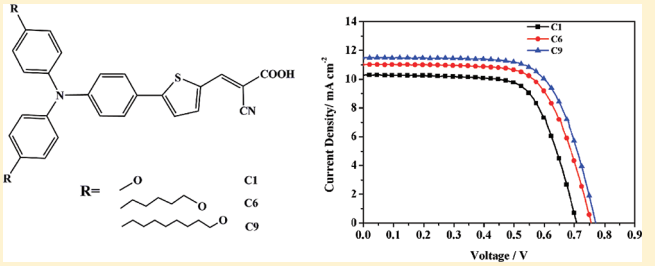

INTRODUCTION

Dye-sensitized solar cells (DSSCs) represent one of the most promising candidates for developing new renewable energy sources due to their low cost and high efficiency.[1] Photosensitizer is one of the key components of DSSCs. Ruthenium-based sensitizers, such as N3,[2] N719,[3] and black dye[4] have achieved efficiencies of up to ~11% under AM 1.5 G irradiation.[5] However, there are still many problems to be addressed in terms of precious ruthenium metal and their high synthetic cost. Therefore, the interests in and the perspectives for cheap alternative metal-free organic sensitizers have drawn great attention.[6] Moreover, high molar extinction coefficients of metal-free organic dyes allow the use of thinner TiO_2 films, which is beneficial for charge separation.[7] Another important advantage over ruthenium-based sensitizers is the availability of versatile functional molecules associated with tuning the electronic and chemical properties. Recently, the DSSCs performance based on organic dye has been remarkably improved and reached impressive efficiencies over 8%.[8,9]

Most of the dipolar organic sensitizers with donor and acceptor segments are bridged by a π-conjugation unit where amine derivatives act as the electron donor, while a 2-cyanoacrylic acid or rhodanine unit acts as the electron acceptor.[10] And possibly the strong electrodonating ability of these donors facilitates intramolecular charge transfer between the donor and the acceptor and leads to a red shift of the absorption.[11] Recently, a novel organic sensitizer, incorporating a hexyloxyl disubstituted triphenyl-amine unit as the electron donor and a dithiophene moiety as the conjugated spacer, yielded very high incident monochromatic photon-to-current conversion efficiency and remarkable stability.[12] One of our strategies to obtain high photovoltaic performance for organic DSSCs is to modify organic dyes in a systematic fashion by varying key components or substituents, because small structural changes of dyes may result in significant difference in the interfacial recombination and absorption behavior of the dyes on TiO_2 surfaces. In this paper, we report three new organic sensitizers (**C1**, **C6**, and **C9**) containing disubstituted triphenyl-amine groups as electron donors and cyanoacrylic acid as an electron acceptor, which are bridged by a thiophene moiety (Scheme 1). The difference of the photovoltaic performance based on these dyes has been analyzed by UV−vis absorption and emission spectra, cyclic voltammograms (CVs), electrochemical impedance spectroscopy (EIS), intensity modulated photocurrent spectroscopy (IMPS), intensity modulated photovoltage spectroscopy (IMVS), and density functional theory (DFT) studies. We show that careful molecular engineering of the dye has an immense influence on the device performance. By incorporating longer alkyl group into the disubstituted triphenyl-amine based dyes, the efficiency can be improved significantly.

Received: June 10, 2011
Revised: September 8, 2011
Published: September 27, 2011

dx.doi.org/10.1021/jp2054519 | J. Phys. Chem. C 2011, 115, 22002–22008

Scheme 1. Molecular Structures of Organic Dyes C1, C6, and C9

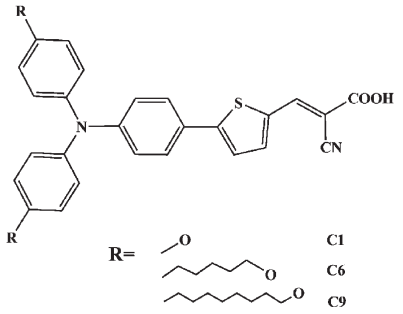

EXPERIMENTAL SECTION

General Methods. All reagents were obtained from commercial sources and used as received. Tetrahydrofuran (THF) was purified using MBRAUN MB SPS-800 system. Other solvents were dried over sodium or calcium hydrides and distilled before used. 4-methoxy-*N*-(4-methoxyphenyl)-*N*-phenylaniline (**1a**), 4-(hexyloxy)-*N*-(4-(hexyloxy)phenyl)-*N*-phenylaniline (**1b**), 4-(nonyloxy)-*N*-(4-(nonyloxy)phenyl)-*N*-phenylaniline (**1c**), 4-bromo-*N*,*N*′-bis(4-methoxy- phenyl)aniline (**2a**), 4-bromo-*N*,*N*′-bis(4-hexyloxyphenyl)aniline (**2b**), 4-bromo-*N*,*N*′-bis(4- nonyloxyphenyl)aniline (**2c**), 5-(4-(bis(4-methoxyphenyl)amino)phenyl)thiophene-2-carbaldehyde (**3a**), 5-(4-(bis(4-hexyloxymethoxyphenyl)-amino)phenyl) thiophene-2-carbaldehyde (**3b**), and 5-(4-(bis(4-nonyloxymethoxyphenyl)amino) phenyl) thiophene-2-carbaldehyde (**3c**) were prepared according to the procedures listed in the Supporting Information (S1).

^{1}H NMR and ^{13}C NMR spectra were recorded on a Mercury-Plus 300FT-NMR spectrometer in DMSO-d_6 or $CDCl_3$, respectively. IR spectra were obtained on a Thermo Scientific Nicolet 330 infrared spectrophotometer. Mass spectroscopy (MS) data were obtained using a LCQ DECA XP liquid chromatography—mass spectrometer. UV—vis absorption spectra were measured using a Shimadzu UV-2450 spectrometer. Emission spectra were measured using Shimadzu RF-5301PC spectrometer. CVs were recorded using a CHI 832 electrochemical analyzer with FTO/TiO_2/Dye as the working electrode, Ag/AgCl as the reference electrode, and Pt wire as the counter electrode. CVs were measured with 0.1 M tetrabutylammonium hexafluorophosphate (Bu_4NPF_6) as a supporting electrolyte in CH_2Cl_2. The scan rate was kept as 50 mV s^{-1} for all compounds. The highest occupied molecular orbital (HOMO) and lowest unoccupied molecular orbital (LUMO) energies of ruthenium complexes obtained from the theoretical calculations were coupled with the redox potentials obtained from the CV measurements as shown in main text.

*Synthesis of 3-(5-(4-(Bis(4-methoxyphenyl)amino)phenyl)-thiophen-2-yl)-2-cyanoacrylic Acid (**C1**).* Compound **3a** (249 mg, 0.6 mmol), cyanoacetic acid (82 mg, 0.96 mmol), and piperidine (0.13 mL, 1.32 mmol) were dissolved in acetonitrile (25 mL) and heated under reflux for 10 h. After being cooled to room temperature, the solution was acidified with 20% aqueous HCl and extracted with chloroform. The organic phase was dried over anhydrous magnesium sulfate. The solvent was removed by rotary evaporation, and the residue was purified on a silica gel column using dichloromethane/methanol (10:1) eluent to give **C1** (133 mg, 46%). ^{1}H NMR (300 MHz, DMSO-d_6) δ (ppm): 8.35 (s, 1H),7.90 (d, J = 3.9 Hz, 1H), 7.57 (d, J = 8.4 Hz, 2H), 7.52 (d, J = 4.2 Hz, 1H), 7.09 (d, J = 8.7 Hz, 4H), 6.94 (d, J = 8.7 Hz, 4H), 6.74 (d, J = 8.7 Hz, 2H), 3.74 (s, 6H). ^{13}C NMR(75 MHz, $CDCl_3$) δ (ppm): 165.7, 150.4, 147.7, 140.6, 139.8, 133.5, 127.5, 123.9, 122.9, 119.2, 115.1, 55.8, 30.1. ESI-MS: m/z 480.8 ([M−H]$^-$). IR (KBr, cm^{-1}): 3430 (ν_{O-H}), 2926 (alkyl ν_{C-H}), 2216 ($\nu_{C\equiv N}$), 1505 ($\nu_{thiophe}$). Elemental Analysis: Calcd for **C1**: C, 69.69; H, 4.6; N, 5.81. Found: C, 69.87; H, 4.54; N, 5.42%.

*Synthesis of 3-(5-(4-(Bis(4-hexylmethoxyphenyl)amino)-phenyl)thiophen-2-yl)-2-cyanoacrylic Acid (**C6**).* The product was synthesized in a similar procedure as described above for **C1**. Yields: 48%. ^{1}H NMR(300 MHz, DMSO-d_6) δ(ppm): 8.37 (s, 1H), 7.91 (d, J = 3.8 Hz, 1H), 7.57 (d, J = 8.5 Hz, 2H), 7.52 (d, J = 4.2 Hz, 1H), 7.07 (d, J = 8.7 Hz, 4H), 6.92 (d, J = 8.8 Hz, 4H), 6.74 (d, J = 8.7 Hz, 2H), 3.95 (t, J = 6.3 Hz, 4H), 1.74 (m, 4H), 1.42 (m, 12H), 0.89 (t, J = 6.1 Hz, 6H). ^{13}C NMR (75 MHz, $CDCl_3$) δ (ppm): 157.1, 156.4, 150.5, 147.7, 140.7, 139.6, 133.4, 127.5, 123.8, 122.9, 119.1, 116.4, 115.7, 68.6, 31.9, 29.7, 26.1, 22.9, 14.4. ESI-MS: m/z 620.8 ([M−H]$^-$). IR (KBr, cm^{-1}): 3431 (ν_{O-H}), 2928 (alkyl ν_{C-H}), 2216 ($\nu_{C\equiv N}$), 1504 ($\nu_{thiophe}$). Elemental Analysis: Calcd for **C6**: C, 73.28; H, 6.8; N, 4.5. Found: C, 73.53; H, 6.70; N, 4.71%.

*Synthesis of 3-(5-(4-(Bis(4-nonylmethoxyphenyl)amino)-phenyl)thiophen-2-yl)-2-cyanoacrylic Acid (**C9**).* The product was synthesized in a similar procedure as described above for **C1**. Yields: 50%. ^{1}H NMR (300 MHz, DMSO-d_6) δ (ppm): 8.37 (s, 1H), 7.91 (d, J = 3.9 Hz, 1H), 7.57 (d, J = 8.8 Hz, 2H), 7.52 (d, J = 4.2 Hz, 1H), 7.07 (d, J = 8.6 Hz, 4H), 6.92 (d, J = 8.7 Hz, 4H), 6.74 (d, J = 8.5 Hz, 2H), 3.94 (t, J = 6.2 Hz, 4H), 1.74 (m, 4H), 1.42 (m, 24H), 0.87 (t, J = 6.3 Hz, 6H). ^{13}C NMR (75 MHz, $CDCl_3$) δ (ppm): 157.2, 156.4, 150.5, 147.9, 140.8, 139.6, 133.4, 127.5, 123.8, 122.9, 119.1, 116.3, 115.7, 68.6, 32.3, 29.9, 29.8, 29.7, 29.6, 26.5, 23.0, 14.5. ESI-MS: m/z 704.9 ([M−H]$^-$). IR (KBr, cm^{-1}): 3431 (ν_{O-H}), 2924, 2853 (alkyl ν_{C-H}), 2217 ($\nu_{C\equiv N}$), 1504 ($\nu_{thiophe}$). Elemental Analysis: Calcd for **C9**: C, 74.75; H, 7.7; N, 3.96. Found: C, 74.88; H, 7.67; N, 3.94%.

TiO_2 electrode was prepared according to the reported literature procedure.[13]

Dye-Loading Measurements. The dye loading measurements on TiO_2 films were carried out by desorbing the dye into 0.8 mol/L triethylamine solution in CH_2Cl_2 and then measuring the ultraviolet—visible absorption spectra of the resultant solution with the same dilution. The adsorbed density of each dye was calculated from the difference concentration of each solution before and after TiO_2 film immersion.

Fabrication of DSSCs. The assembly of the DSSCs: TiO_2 films with 15 μm in thickness were prepared by following the literature procedure[14] and soaked in 40 mM $TiCl_4$ aqueous solution at 70 °C, which improved the photocurrent and photovoltaic performance of DSSCs. After 30 min, the TiO_2 films were washed with water and ethanol and then sintered at 520 °C for 30 min. After cooling to 80 °C, the $TiCl_4$-treated TiO_2 electrodes were immersed into 0.3 mM $CHCl_3$ solution of the organic dye and kept at room temperature for 16 h. The active area of the dye-coated TiO_2 film was 0.16 cm^2, which was measured by profilometer (AMBIOS, XP-1).

Characterization of DSSCs. The current—voltage characteristics were measured by using a Keithley 2400 source meter under simulated AM 1.5 G one sun (100 mW cm^{-2}) illumination provided by solar simulator (91192, 1 kW Xe lamp with optical filter, Oriel). The volatile electrolyte solution is composed of 0.6 M 1-propyl-3-methylimidazolium iodide (PMII), 0.03 M iodine,

Scheme 2. Synthetic Routes to the Dyes C1, C6, and C9

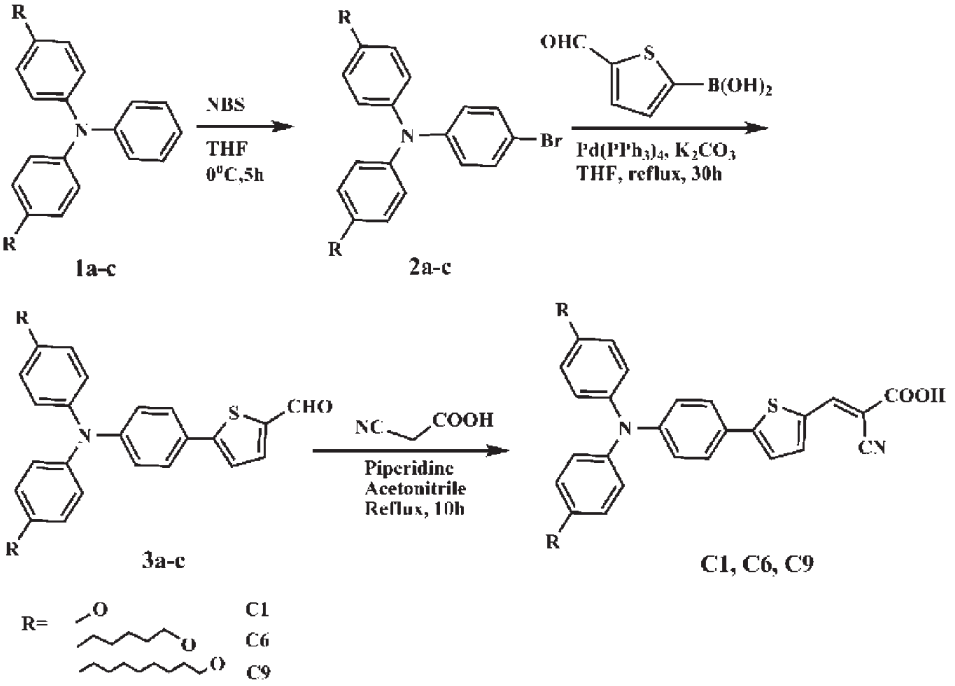

0.05 M LiI, 0.1 M guanidinium thiocyanate (GuSCN), and 0.5 M 4-tert-butylpyridine (TBP) in acetonitrile and valeronitrile (85:15 v/v). The nonvolatile electrolyte contains 1.0 M PMII, 0.15 M iodine, 0.1 M GuNCS, and 0.5 M *N*-methylbenzimidazole (NMB) in 3-methoxypropionitrile (MPN).[5e] The incident photon-to-current conversion efficiencies (IPCEs) spectra were measured as a function of wavelength from 350 to 700 nm on the basis of a Spectral Products DK240 monochromator.

EIS. The EIS measurements were performed with a Zennium electrochemical workstation (ZAHNER) with the frequency range from 10 mHz to 1000 kHz. The magnitude of the alternative signal was 10 mV. The impedance measurements were carried out under forward bias of −0.65 V in the dark.

Electron Transport and Electron Lifetime Measurements. IMPS and IMVS measurements were conducted using electrochemical workstation (ZAHNER, Zennium) and were performed under a modulated LED light (457 nm) driven by a source supply (ZAHNER, PP210). The illumination intensity ranged from 30 to 150 mW cm^{-2}. The light intensity modulation was 20% of the base light intensity over the frequency range of 10^{-1}−10^{3} Hz.

Computational Method. Density fuctional theory (DFT) at the hybrid Becke, three-parameter Lee−Yang (B3LYP) level and the CPCM solvent model were used to optimize the geometries of the model complexes. The Los Alamos effective core potentials (ECPs) on Ru were used to replace the inner core electrons, while the DZ basis set was applied to describe the outer core ($4s^2 4p^6$) and the valence 4d electrons (LANL2DZ). For all the other atoms (C, H, O, N, and S), the 6-31G* basis set was used. All the calculations were carried out with the Gaussian09 software package.

RESULTS AND DISCUSSION

Scheme 2 illustrates the synthetic protocol of three organic sensitizers **C1**, **C6**, and **C9**. The disubstituted triphenyl-amine bromides **2a**−**c** were synthesized by bromination of **1a**−**c** with *N*-bromosuccinimide (NBS) in THF. The attachment of 5-formyl-2-thiophene unit to **2a**−**c** was achieved by the Suzuki coupling reaction of **2a**−**c** with 5-formyl-2-thiopheneboronic acid, giving **3a**−**c**. The final Knoevenagel condensation of the aldehyde **3a**−**c** with cyanoacetic acid in the presence of piperidine in CH_3CN yielded the three organic sensitizers. The molecular structure of these dyes was confirmed by various spectroscopic methods such as NMR, mass spectra, and elemental analysis.

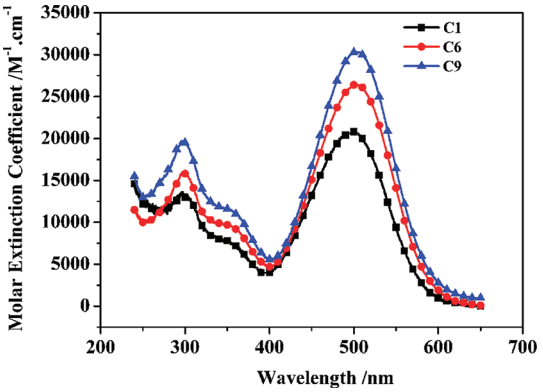

Figure 1. Absorption spectra of **C1** (black), **C6** (red), and **C9** (blue) in CH_2Cl_2 solution.

Figure 1 shows the UV−vis spectra of three organic dyes, **C1**, **C6**, and **C9**, measured in dichloromethane solutions. The absorption spectrum of the **C1** dye displays a strong visible band at 499 nm (ε = 20600 M^{-1} cm^{-1}) due to π−π^* charge transfer transitions of the conjugated molecule. The **C6** and **C9** dyes also exhibit similar spectral properties (absorption maxima at 503 and 504 nm, ε = 26400 and 30300 M^{-1} cm^{-1}, respectively). It is clear that the absorption wavelength (λ_{max}) and molar extinction

dx.doi.org/10.1021/jp2054519 |*J. Phys. Chem. C* 2011, 115, 22002–22008

coefficient of three dyes normally increase with increasing alkyl chain length, in accordance with the literature that studied dyes with similar substituents.[15] The red-shift and enhanced molar extinction coefficient may favor light harvesting and hence photocurrent generation in DSSCs. We assume that the reason of this higher absorption coefficient lies in the extension of the C chain, and the longer hydrophobic hydrocarbon isolating chain might act as the better absorber material for the incoming light.

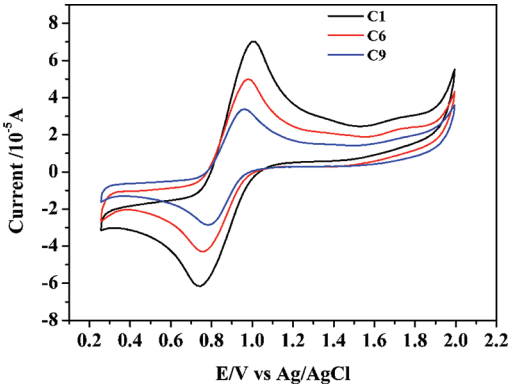

Figure 2. CVs of **C1** (black line), **C6** (red line), and **C9** (blue line) on TiO_2. 0.1 M $TBAPF_6$ in CH_2Cl_2 was used as the supporting electrolyte (working electrode: FTO/TiO_2/dye; reference electrode: Ag/AgCl; counterelectrode: Pt; scan rate: 50 mV/s).

In common with many metal-free dyes, there is blue shift of the absorption peak in more polar solvents (Figure S1−S3). This may be attributed to the strong interaction of polar solvent molecules with the dyes, which weakens the O−H bond of the carboxylic acid and consequently decreases the electron-withdrawing nature of the COOH group.[16] In addition, the broadening of the dyes adsorption on the surface of the TiO_2 films and red shift of the peak maxima is believed to result from the formation of J-aggregates (Figure S4).[16]

To evaluate the possibility of electron transfer from the excited dye molecule to the conductive band of TiO_2, the CV of three dyes was measured in dichloromethane (CH_2Cl_2) with 0.1 M tetrabutylammonium hexafluorophosphate ($TBAPF_6$) as supporting electrolytes and TiO_2 films anchored with the dyes as working electrodes (Figure 2). The ferrocene was used as a calibration internal standard, and the $E_{1/2}$ of the Fc/Fc^+ redox couple was found to be 0.65 V vs the Ag/AgCl reference electrode. Electrochemical oxidation potentials of **C1**, **C6**, and **C9** on TiO_2 films were recorded, and their values are listed in Table 1. The first oxidation potentials of the dyes (**C1**: 0.58; **C6**: 0.55; **C9**: 0.53 V vs NHE (normal hydrogen electrode)) are more positive than the I^-/I_3^- redox couple (∼ 0.4 V vs NHE), providing a thermodynamic driving force for efficient dye regeneration. The reduction potentials of three sensitizers calculated from the oxidation potentials and the E_{0-0} determined from the intersection of normalized absorption and emission spectra are listed in Table 1. The excited-state redox potentials, which

Table 1. Optical, Redox, and DSSC Performance Parameters of Dyes

dye	$\varepsilon/10^4$ M^{-1} cm^{-1} (λ_{max}/nm)	λ_{em}/nm	$^aE_{ox}$/V (vs NHE)	$^bE_{0-0}$/ eV	$^cE_{LUMO}$/V (vs NHE)	amounts/ 10^{-7} mol cm^{-2}	J_{sc}/ mA cm^{-2}	V_{oc}/ mV	*FF*	η (%)
C1	2.06 (499)	513	0.58	2.37	−1.79	2.2	10.29	707	0.69	4.99
C6	2.64 (503)	514	0.55	2.36	−1.81	1.9	11.00	756	0.68	5.64
C9	3.03 (504)	516	0.53	2.35	−1.82	1.6	11.48	770	0.68	6.04

[a] E_{ox} is the oxidation potential. The redox potential of dyes on TiO_2 was measured in DMF with 0.1 M $TBAPF_6$ at a scan rate of 50 mV s^{-1} (vs Fc/Fc^+). [b] E_{0-0} was determined from the intersection of absorption and emission spectra in methanol. [c] $E_{LUMO} = E_{ox} - E_{0-0}$. Performances of DSSCs were measured with 0.16 cm^2 working area.

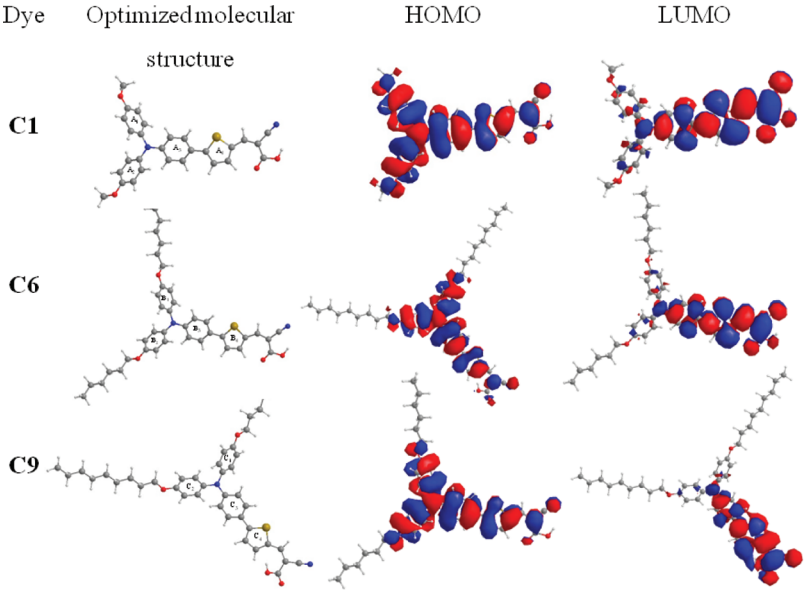

Figure 3. Frontier molecular orbitals (HOMO and LUMO) of **C1**, **C6**, and **C9** calculated with DFT on the B3LYP/6-31G* level.

dx.doi.org/10.1021/jp2054519 |*J. Phys. Chem. C* 2011, 115, 22002–22008

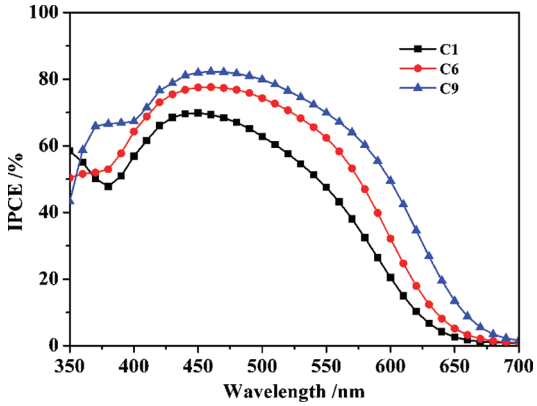

Figure 4. The IPCEs spectra for DSSCs sensitized with **C1**, **C6**, and **C9**. black: **C1**, red: **C6**, and blue: **C9**.

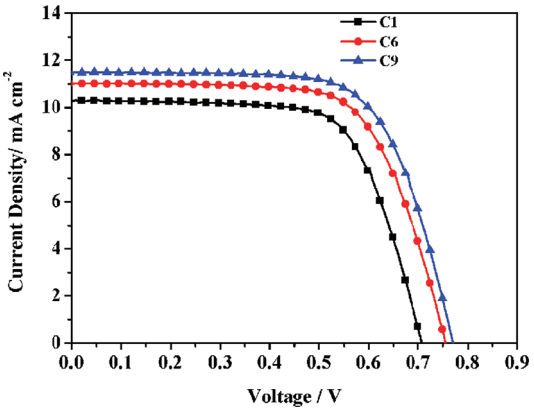

Figure 5. Photocurrent density versus voltage curves for DSSCs sensitized with **C1**, **C6**, and **C9** under AM 1.5 G one sun solar light (100 mW cm^{-2}). black: **C1**, red: **C6**, and blue: **C9**.

correspond to the LUMO of three dyes (**C1**: −1.79 V; **C6**: −1.81 V; **C9**: −1.82 V vs NHE), are more negative than the conduction band of TiO_2 (at approximately −0.5 V versus NHE), indicating that the electron injection process is energetically favorable. It is worth noting that the LUMO energy levels of **C9** and **C6** are more negative than the conduction band of TiO_2 relative to **C1**, indicative of the more significant driving force for charge injection. These findings denote that the long alkyl chains in **C6** and **C9** dyes could tune the localization of the frontier orbitals appropriately and enhance the driving force for charge injection, thus making the device performance of **C9** and **C6** superior to that of **C1**.

To scrutinize the geometrical and photophysical properties, molecular orbital calculations of **C1**, **C6**, and **C9** were carried out using the TD-DFT and B3LYP/3-21G* program. The calculation shows the HOMOs of these dyes largely populate on the disubstituted triphenyl-amine moiety as well as the thienyl conjugation unit, indicating the donor ability of disubstituted triphenyl-amine group in these dyes. The LUMOs of these dyes are delocalized over the cyanoacrylic and thienyl unit with a sizable contribution on the far end cyanoacrylic unit, such that the excited electron can be injected into the TiO_2 electrode effectively (Figure 3). Preliminary TDDFT computations (Figure S5 and Table S1) also highlight the electrondonating character of disubstituted triphenyl-amine moiety toward excitation. The two lowest-lying electronic transitions, S1 (mainly HOMO→LUMO) and S2 (mainly HOMO-1→LUMO), have significant oscillator strength (f) and extent of charge separation (i.e., changes in Mulliken charge in the transition) from the disubstituted triphenyl-amine to the 2-cyanoacrylic acid. This is consistent with the experimental results.

The IPCEs for DSSCs based on the three dyes are shown in Figure 4. The IPCE curves for the **C1**-, **C6**-, and **C9**-containing DSSCs exhibited broad absorption in the range of 350−700 nm, with maxima at 69.8, 77.6, and 82.2% respectively. The enhanced IPCE spectra of **C6** and **C9** suggest that these new dyes containing the long alkyl chains might act as more efficient electron donors to the conduction band of the TiO_2 film upon photoexcitation.

The current density−voltage (I−V) characteristic of the photovoltaic devices containing **C1**, **C6**, and **C9** is shown in Figure 5 with detailed photovoltaic parameters listed in Table 1. Under a standard global AM 1.5 G one sun solar illumination, **C1** and **C6** sensitized solar cells give short circuit photocurrent densities (J_{sc}) of 10.29 and 11.00 mA cm^{-2}, open circuit voltages (V_{oc}) of 707 and 756 mV, and fill factors (FF) of 0.69 and 0.68, corresponding to overall conversion efficiencies (η) of 4.99 and 5.64%, respectively. Under the same condition, the **C9** sensitized solar cell gives a J_{sc} of 11.48 mA cm^{-2}, a V_{oc} of 770 mV, and an FF of 0.68, corresponding to η of 6.04%. These observations indicate the short circuit photocurrent as well as the open circuit voltage increase significantly with the increasing of chain length, leading to a linear increment in device efficiency with chain length. To clarify the influence of the hydrophobic hydrocarbon chain length of the dyes on the device performance, we have measured the amount of dyes adsorbed on TiO_2 film. As seen from Table 1, the adsorbed amounts of 2.2×10^{-7} mol cm^{-2} for **C1**, 1.9×10^{-7} mol cm^{-2} for **C6**, and 1.6×10^{-7} mol cm^{-2} for **C9** are slightly decreasing. Therefore, it is obvious that the enhanced J_{sc} in the dyes with longer alkyl chains is not originated from their adsorbed amounts. Of particular importance is the 49 and 63 mV increase in V_{oc} of **C6**- and **C9**-based cell relative to the **C1**-based cell, which clearly suggests that the long hydrophobic hydrocarbon chains in **C6** and **C9** can effectively enhance the device performance. We attribute these behaviors to the following reasons: the long hydrophobic alkyl chains of the dyes can facilitate self-assembly of the dyes into layers, which are apt to extend between the TiO_2 film and the I_3^-/ I^- electrolyte, thus blocking the recapture of the photoinjected electrons by triiodide ions. In addition, lengthening of the alkyl chains of the dyes could lead to a longer distance between the TiO_2 layer and the electrolyte. Therefore, the chain length exerts a strong influence on the blocking behavior of the dyes, explaining why the longer the hydrocarbon chain is, the higher the efficiency observed for the cells.

To investigate the effect of the length of the alkyl chains on the overall solar cell performance using more viscous electrolyte, the photovoltaic performance measurements of **C1**, **C6**, and **C9**-sensitized solar cells based on a nonvolatile organic solvent electrolyte (composition stated in Experimental Section) were carried out. The photovoltaic parameters J_{sc}, V_{oc}, FF, and η for **C9**-sensitized DSSCs devices in the presence of this nonvolatile and more viscous electrolyte are 10.98 mA cm^{-2}, 737 mV, 0.67, and 5.46%, respectively. Using **C1** and **C6** dyes with the same nonvolatile electrolyte, 4.36% and 4.97% efficiencies were obtained, respectively (Figure S7, Supporting Information). The detailed photovoltaic parameters for different dyes are shown in Table S2. The results indicate that the dyes with longer

dx.doi.org/10.1021/jp2054519 |J. Phys. Chem. C 2011, 115, 22002–22008

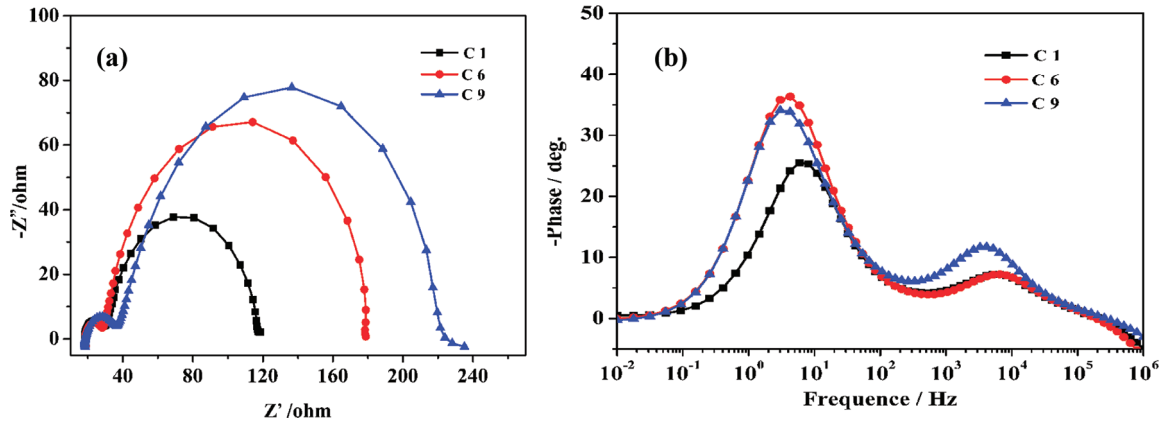

Figure 6. (a) EIS Nyquist plots (i.e., minus imaginary part of the impedance $-Z''$ versus the real part of the impedance Z' when sweeping the frequency) and (b) EIS Bode plots (i.e., the phase of the impedance vs the frequency) for DSSCs sensitized with **C1**, **C6**, and **C9** dyes. black: **C1**, red: **C6**, and blue: **C9**.

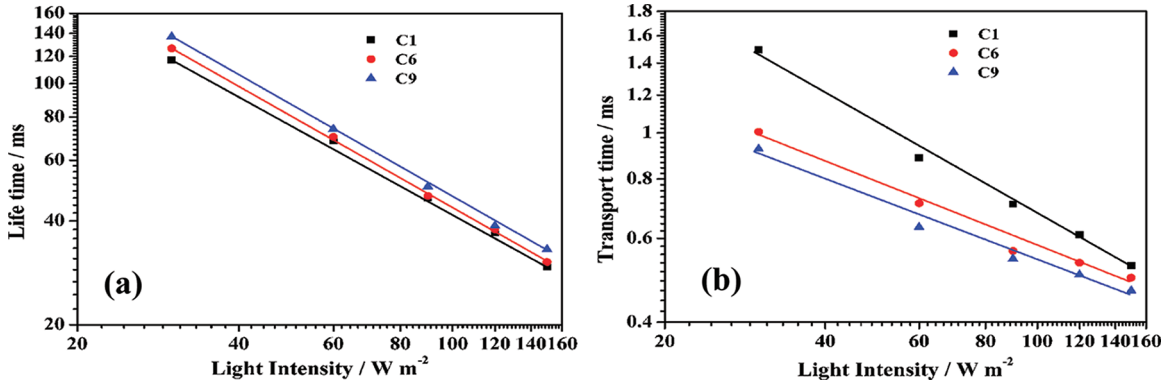

Figure 7. (a) Incident light intensity-dependent recombination time constants, (b) incident light intensity-dependent transport time constants. black: **C1**, red: **C6**, and blue: **C9**.

hydrocarbon chains also give higher efficiency in more viscous electrolyte such as MPN, which is consistent with the previous reports on the dyes with different hydrocarbon chains for ionic liquid based[16b] or solid-state dye-sensitized[15] solar cells.

EIS analyses were also performed to elucidate above photovoltaic findings. The Nyquist plots (Figure 6a) show the radius of the middle semicircle to increase in the order **C1** < **C6** < **C9**, indicating that the electron recombination resistance augments from **C1** to **C9**. The electron lifetime values derived from curve fitting are 53.4, 101.4, and 114.1 ms, respectively. The longer the hydrophobic hydrocarbon chain is, the higher increase in electron lifetime. This strongly supports the speculation that the long hydrophobic alkyl chain can act as an effective blocking spacer between the TiO_2 layer and the electrolyte, leading to more effective suppression of the back reaction of the injected electron with the I_3^- in the electrolyte, which is reflected in the improved photocurrent and photovoltage, yielding substantially enhanced device efficiency.

The Bode phase plots shown in Figure 6b likewise support the differences in the electron lifetime for TiO_2 films derivatized with the three dyes. The middle-frequency peaks of the DSSCs based on **C6** and **C9** shift to lower frequency relative to that of **C1**, indicating a shorter recombination lifetime for the latter species. The increase in the recombination lifetime in the TiO_2 film is associated with a pronounced rise in the charge transfer resistance, implying that the long alkyl chains in **C6** and **C9** decrease the interfacial rate constant for electron capture by the I_3^- ions. In addition, at high frequency region (10^3–10^6 Hz), the peak maximum is at slightly lower frequency for **C9** than the other two dyes, which corresponds to the slower charge transfer at counter electrode.

IMPS and IMVS were carried out to further investigate the different photovoltaic behaviors of three dyes. Figure 7a shows recombination times (τ_r) of DSSCs based on **C1**, **C6**, and **C9** dyes under various incident light intensities. The results indicate that the recombination times of the devices display a systematic trend **C9** > **C6** > **C1**, consistent with the EIS results described above. On the other hand, the electron transport times (τ_d) of DSSCs based on the three dyes increase in the order **C1** > **C6** > **C9**, as shown in Figure 7b, which is in accordance with the current density–voltage (I–V) characteristic results. Considering the order of LUMO values, **C1** > **C6** > **C9**, it is understandable that the most negative LUMO energy level of **C9** among these three dyes ensures the highest driving force for charge injection, thus resulting in the fastest photoinjected electron transport to back contact. In addition, the charge collection efficiencies (η_{cc}) determined by IMPS/IMVS through the equation $\eta_{cc} = 1 - \tau_d/\tau_r$ are shown in Figure S6. The results indicate that the charge collection efficiency increases in the order **C9** > **C6** > **C1**, which is in agreement with the cell performance of the same order.

According to above analyses, the device efficiencies derived from I–V curves, the electron lifetimes obtained in EIS, and the

dx.doi.org/10.1021/jp2054519 |J. Phys. Chem. C 2011, 115, 22002–22008

charge collection efficiencies calculated from in IMVS and IMPS are all in the order of **C9** > **C6** > **C1**. It is thus reasonable to conclude that the broader spectral response, the higher molar absorption coefficient, the slower recombination of photoinjected electrons, and the more appropriate localization of the frontier orbitals account for the higher conversion efficiency for **C9**-based cell in comparison to those of **C1**- and **C6**-based cells.

CONCLUSIONS

In summary, we have synthesized a series of metal-free organic sensitizers based on disubstituted triphenyl-amine, and studied the influence of the hydrophobic hydrocarbon chain length of the substituent group on the device performance in DSSCs. The power-conversion efficiency of DSSCs based on **C9** sensitizer with a nonyloxyl chain (6.04%) is higher than those of **C6** with a hexyloxyl chain (5.64%) and **C1** with a methoxyl moiety (4.99%). Our data reveal that a hydrophobic chain attached to the dye can be used to suppress recombination, enhance the molar absorption coefficient of metal-to-ligand charge transfer (MLCT), and tune the molecular orbitals efficiently. In addition, lengthening of the anchoring groups of the dye could lead to a better absorber for the incoming light and longer blocking layer to avoid charge recombination, thus dramatically improving efficiency and performance of DSSCs devices. These findings strongly suggest that the optimization of absorption character coupled with the minimization of charge recombination represent a key issue associated with the general guideline for designing organic dyes with high sensitization capability in DSSCs.

ASSOCIATED CONTENT

Supporting Information. Synthesis of compounds **1a**−**c**, **2a**−**c** and **3a**−**c**. Absorption spectra of **C1**, **C6**, and **C9** in different solvents. The computed absorption spectra of **C1**, **C6**, and **C9**. Selected calculated singlet excited-state transitions for **C1**, **C6**, and **C9**. The charge collection efficiencies of **C1**, **C6**, and **C9** calculated from IMPS and IMVS. This information is available free of charge via the Internet at http://pubs.acs.org.

AUTHOR INFORMATION

Corresponding Author

*Tel: +86-20-84115178. Fax: +86-20-84115178. E-mail: cesscy@mail.sysu.edu.cn; liujunm@mail.sysu.edu.cn.

ACKNOWLEDGMENT

This work was supported by the 973 Program of China (2012CB821700), NSFC Projects (20821001, 20731005, U0934003), the RFDP of Higher Education of China, and the Fundamental Research Funds for the Central Universities.

REFERENCES

(1) (a) O'Regan, B.; Grätzel, M. *Nature* **1991**, *353*, 737. (b) Hagfeldt, A.; Grätzel, M. *Acc. Chem. Res.* **2000**, *33*, 269. (c) Grätzel, M. *Nature* **2001**, *414*, 338.

(2) Grätzel, M. *J. Photochem. Photobiol. A* **2004**, *168*, 235.

(3) Nazeeruddin, M. K.; Kay, A.; Rodicio, L.; Humphry-Baker, R.; Müller, E.; Liska, P.; Vlachopoulos, N.; Grätzel, M. *J. Am. Chem. Soc.* **1993**, *115*, 6382.

(4) Nazeeruddin, M. K.; Péchy, P.; Renouard, T.; Zakeeruddin, S. M.; Humphry-Baker, R.; Comte, P.; Liska, P.; Cevey, L.; Costa, E.; Shklover, V.; Spiccia, L.; Deacon, G. B.; Bignozzi, C. A.; Grätzel, M. *J. Am. Chem. Soc.* **2001**, *123*, 1613.

(5) (a) Nazeeruddin, M. K.; Kay, A.; Rodicio, L.; Humphry-Baker, R.; Müller, E.; Liska, P.; Vlachopoulos, N.; Grätzel, M. *J. Am. Chem. Soc.* **1993**, *115*, 6382. (b) Chiba, Y.; Islam, A.; Watanabe, Y.; Komiya, R.; Koide, N.; Han, L. *Jpn. J. Appl. Phys.* **2006**, *45*, L638. (c) Qin, P.; Zhu, H.-J.; Edvinsson, T.; Boschloo, G.; Hagfeldt, A.; Sun, L.-C. *J. Am. Chem. Soc.* **2008**, *130* (27), 8570. (d) Nazeeruddin, M. K.; Péchy, P.; Renouard, T.; Zakeeruddin, S. M.; Humphrey-Baker, R.; Comte, P.; Liska, P.; Cevey, L.; Costa, E.; Shklover, V.; Spiccia, L.; Deacon, G. B.; Bignozzi, C. A.; Grätzel, M. *J. Am. Chem. Soc.* **2001**, *123*, 1613. (e) Kuang, D. B.; Klein, C.; Ito, S.; Moser, J.-E.; Humphry-Baker, R.; Evans, N.; Duriaux, F.; Grätzel, C.; Zakeeruddin, S. M.; Grätzel, M. *Adv. Mater.* **2007**, *19*, 1133.

(6) (a) Mishra, A.; Fischer, M. K. R.; Bäuerle, P. *Angew. Chem., Int. Ed.* **2009**, *48*, 2474. (b) Heredia, D.; Natera, J.; Gervaldo, M.; Otero, L.; Fungo, F.; Lin, C.-Y.; Wong, K.-T. *Org. Lett.* **2010**, *12*, 12. (c) Jiang, X.; Marinado, T.; Gabrielsson, E.; Hagberg, D. P.; Sun, L.; Hagfeldt, A. *J. Phys. Chem. C* **2010**, *114*, 2799. (d) Teng, C.; Yang, X.; Yang, C.; Li, S.; Cheng, M.; Hagfeldt, A.; Sun, L. *J. Phys. Chem. C* **2010**, *114*, 9101. (e) Lin, L.-Y.; Tsai, C.-H.; Wong, K.-T.; Huang, T.-W.; Wu, C.-C.; Chou, S.-H.; Lin, F.; C, S.-H.; Tsai, A.-I. *J. Mater. Chem.* **2011**, *21* (16), 5950.

(7) (a) Zeng, W.-D.; Cao, Y.-M.; Bai, Y.; Wang, Y.-H.; Shi, Y.-S.; Zhang, M.; Wang, F.-F.; Pan, C.-Y.; Wang, P. *Chem. Mater.* **2010**, *22* (5), 1915. (b) Feldt, S. M.; Gibson, E. A.; Gabrielsson, E.; Sun, L.-C.; Boschloo, G.; Hagfeldt, A. *J. Am. Chem. Soc.* **2010**, *132* (46), 16714.

(8) (a) Hwang, S.; Lee, J. H.; Park, C.; Lee, H.; Kim, C.; Park, C.; Lee, M.-H.; Lee, W.; Park, J.; Kim, K.; Park, N.-G.; Kim., C. *Chem. Commun.* **2007**, 4887. (b) Qin, H.; Wenger, S.; Xu, M.; Gao, F.; Jing, X.; Wang, P.; Zakeeruddin, S. M.; Grätzel, M. *J. Am. Chem. Soc.* **2008**, *130*, 9202. (c) Paek, S.; Choi, H.; Lee, C.-W.; Kang, M.-S.; Song, K.; Nazeeruddin, M. K.; Ko, J. *J. Phys. Chem. C* **2010**, *114*, 14646.

(9) (a) Zhang, G.-L.; Bala, H.; Cheng, Y.-M.; Shi, D.; Lv, X.-J.; Yu, Q.-J.; Wang, P. *Chem. Commun.* **2009**, 2198. (b) Hagfeldt, A.; Boschloo, G.; Sun, L. C.; Kloo, L.; Pettersson, H. *Chem. Rev.* **2010**, *110*, 6595.

(10) (a) Wiberg, J.; Marinado, T.; Hagbergy, D. P.; Sun, L.; Hagfeldt, A.; Albinsson, B. *J. Phys. Chem. C* **2009**, *113*, 3881. (b) Tian, H.; Yang, X.; Cong, J.; Chen, R.; Liu, J.; Hao, Y.; Hagfeldt, A.; Sum, L. *Chem. Commun.* **2009**, 6288. (c) Wang, Z. S.; Cui, Y.; Hara, K.; Dan-oh, Y.; Kasada, C.; Shinpo, A. *Adv. Mater.* **2007**, *19*, 1138. (d) Chen, R.; Yang, X.; Tina, H.; Wang, X.; Hagfeldt, A.; Sun, L. *Chem. Mater.* **2007**, *19*, 4007. (e) Sayama, K.; Hara, K.; Mori, N.; Satsuki, M.; Suga, S.; Tsukagoshi, S.; Abe, Y.; Sugihara, H.; Arakawa, H. *Chem. Commun.* **2000**, 1173. (f) Hara, K.; Kurashige, M.; Ito, S.; Shinpo, A.; Suga, S.; Sayama, K.; Arakawa, H. *Chem. Commun.* **2003**, 252. (g) Kim, D.; Song, K.; Kang, M. S.; Lee, J. W.; Kang, S. O.; Ko, J. *J. Photochem. Photobiol., A* **2009**, *201*, 102. (h) Biak, C.; Kim, D.; Kang, M. S.; Song, K.; Kang, S. O.; Ko, J. *Tetrahedron* **2009**, *65*, 5302.

(11) (a) Hagberg, D. P.; Jiang, X.; Gabrielsson, E.; Linder, M.; Marinado, T.; Brinck, T.; Hagfeldt, A.; Sun, L. J. *Mater. Chem.* **2009**, *19*, 7232. (b) Im, H.; Kim, S.; Park, C.; Jang, S. H.; Kim, C. J.; Kim, K.; Park, N. G.; Kim, C. *Chem. Commun.* **2010**, 1335. (c) Salice, P.; Arnbjerg, J.; Pedersen, B. W.; Toftegaard, R.; Beverina, L.; Pagani, G. A.; Ogilby, P. R. *J. Phys. Chem. A* **2010**, *114*, 2518.

(12) Lei, B. X.; Fang, W. J.; Hou, Y. F.; Liao, J. Y.; Kuang, D. B.; Su, C. Y. *J. Photochem. Photobiol. A* **2010**, *216*, 8.

(13) Yum, J.-H.; Hagberg, D. P.; Moon, S.-J.; Karlsson, K. M.; Marinado, T.; Sun, L.; Hagfeldt, A.; Nazeeruddin, M. K.; Grätzel, M. *Angew. Chem., Int. Ed.* **2009**, *48*, 1576.

(14) (a) Lei, B. X.; Fang, W. J.; Hou, Y. F.; Liao, J. Y.; Kuang, D. B.; Su, C. Y. *J. Photochem. Photobiol. A* **2010**, *216*, 8. (b) Qu, S. Y.; Wu, W. J.; Hua, J. L.; Kong, C.; Long, Y. T.; Tian, H. *J. Phys. Chem. C* **2010**, *114*, 1343.

(15) Schmidt-Mende, L.; Eroeze, J. K.; Durrant, J. R.; Nazeeruddin, M. K.; Grätzel, M. *Nano Lett.* **2005**, *5* (7), 1315.

(16) (a) Yang, H.-Y.; Yen, Y. S.; Chou, Y.-C.; Lin, J. T. *Org. Lett.* **2010**, *12* (1), 16. (b) Kuang, D.-B.; Uchida, S.; Humphrry-Baker, R.; Zakeeruddin, S. M.; Grätzel, M. *Angew. Chem., Int. Ed.* **2008**, *47*, 1923.